

Wettability Contrast Gravure Printing

Heng Zhang, Alexander Ramm, Sooman Lim, Wei Xie, Bok Yeop Ahn, WeiChao Xu, Ankit Mahajan, Wieslaw J. Suszynski, Chris Kim, Jennifer A. Lewis, C. Daniel Frisbie,* and Lorraine F. Francis*

Flexible electronic circuits and devices have a diverse range of potential applications, including energy generation and storage, health-care diagnostics, human-machine interfaces, and consumer electronic displays and devices. Creating circuits on flexible substrates, such as plastic and paper, is arguably best achieved by additive printing processes that are low cost, scalable, and fast. Several contact-based printing techniques, including gravure printing, flexographic printing, and screen printing, as well as nozzle-based methods, such as inkjet printing and aerosol jet printing, have been studied for flexible electronics applications. Among them, gravure printing is a fast, roll-to-roll, commercial technique that is typically used to print high volume products, such as magazines. With the development of electrically functional inks, gravure printing is also emerging as a viable method for fabricating flexible electronics.^[1–11]

A gravure printing system is composed of two cylinders: an engraved gravure roll, which is patterned with many small, recessed cells, and an impression or backing roll. The cells are typically patterned into the surface of a metal cylinder by mechanical or chemical etching, or laser cutting; however, even using the most sophisticated approach, it is difficult to achieve features below 10 μm . Only one report in the literature^[4] demonstrates resolution under 10 μm with gravure rolls made by engraving techniques. During printing, ink is applied to the gravure roll from an ink tray, and excess ink is removed by a doctor blade that ideally leaves ink only in the recessed cells. When the gravure roll comes into contact with a plastic or paper substrate that is fed between the two rolls, the ink is transferred from the cells to the substrate. To improve the printing resolution, small gravure cells are needed along with optimization of the interaction between ink and substrate. Subramanian and coworkers^[12–14] recently achieved very high resolution (<2 μm)

using etched silicon wafers as gravure plates. They also noted that fully removing the ink from the nonimage areas or 'lands' between the cells is challenging due to the persistence of thin lubrication layer of ink^[13] and that the thickness of the lubrication layer can be minimized with proper selection of the doctor blade configuration, ink properties, and speed.^[15]

Here, we report a new method for creating functionalized gravure rolls that obviates the need for physical doctoring and presents an alternative approach to gravure printing. Specifically, we create patterns using photolithographic techniques on a thin flexible silicon wafer, which can later be wrapped around a metal cylinder, as shown in **Figure 1c**. The advantages of this strategy are twofold: first, extremely precise and reliable patterns down to below 1 μm can be achieved, and second, functionalizing the surface of the pattern enhances the wettability contrast between the cells and the surrounding lands, allowing excess ink to be removed without using a doctor blade.

The silicon gravure pattern is produced by standard photolithography and etching processes together with selective surface functionalization designed for printing of aqueous-based inks (**Figure 1a**). We explored ink filling and printing using model inks composed of water/glycerol solution, as well as silica and silver nanoparticle-based inks. As shown in **Figure 1b**, the gravure pattern consists of hydrophilic cells and hydrophobic lands. The wettability contrast is facilitated by a nickel layer inside the silicon gravure cell as well as a fluorinated layer on the surface of the lands, created using a self assembled monolayer, trichloro(1H,1H,2H,2H-perfluorooctyl)silane (FOTS). The contact angle, θ , of water on the FOTS-treated silicon surface is 110°. In the process sequence, the gold layer protects the nickel from exposure to FOTS; in the last process step the gold is etched away to leave behind a wettable nickel cell interior. With the use of the gold protecting layer, the contact angle between water and nickel cell interior is 30°, leading to a wettability contrast $\Delta\theta$ of 80°. Without the protectant, $\Delta\theta$ is only 50°. To apply the silicon pattern to 5" diameter gravure roll, the wafer must be $\approx 100 \mu\text{m}$ thick. Appropriately thin wafers are prepared by chemical etching and robust wrapping techniques have been reported.^[16] Alternatively, printing can be accomplished by feeding a silicon pattern between two counter-rotating rolls with the substrate wrapped on the backing roll (**Figure 1d**).

To probe the influence of wettability contrast on cell filling, ink is either introduced in a dropwise or layer fashion over the Si gravure pattern or the pattern is withdrawn from an ink reservoir using a dip-coating system. **Figure 2a,b** shows two images in a time sequence for filling a model water/glycerol solution ink using the guided drop method. The droplet travelled from the lower left to the upper right corner and filled the recessed

Dr. H. Zhang, A. Ramm, Dr. S. Lim,
Dr. W. Xie, W. Xu, A. Mahajan,
W. J. Suszynski, Prof. C. Kim,
Prof. C. D. Frisbie, Prof. L. F. Francis
Department of Chemical Engineering
and Materials Science
University of Minnesota
421 Washington Avenue
S.E. Minneapolis, MN 55455, USA
E-mail: frisbie@umn.edu; lfrancis@umn.edu

Dr. B. Y. Ahn, Prof. J. A. Lewis
School of Engineering and Applied Sciences
Wyss Institute for Biologically Inspired Engineering
Harvard University
Cambridge, MA 02318, USA

DOI: 10.1002/adma.201502639



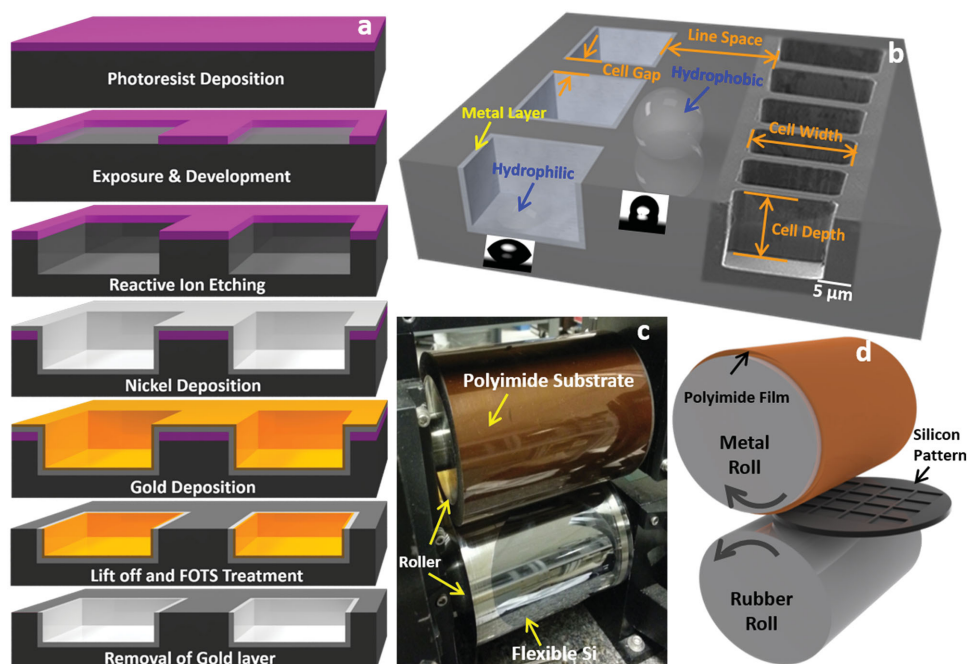


Figure 1. a) Schematic drawing of wettability contrast pattern fabrication procedure. The step of adding the gold layer to protect the nickel surface during silane exposure was developed based on initial results. b) Schematic drawing showing the wettability contrast with a hydrophobic surface on the land and hydrophilic surface in the cell. The incorporated SEM image was taken from a real pattern. Photos showing water drops and contact angles with the interior of the cell and the land are also included. c) Two-roll gravure printing system. A polyimide substrate is wrapped around the upper backing roll and a patterned flexible silicon wafer is wrapped around the lower roll (gravure roll). d) Schematic drawing of flat patterned wafer printing. Polyimide film was wrapped around the metal roller, a flat ink-loaded patterned silicon wafer was passed through two rollers and the printing speed is controlled by a computer.

hydrophilic cells, leaving no residual ink on the hydrophobic lands (see Video S1, Supporting Information). The liquid front is momentarily pinned at the cell edges due to geometry and chemical heterogeneity between the cell and the land. With enough stretching, the liquid front jumps to the next cell, dewetting the flat surface between cells. Ink filling by dip coating, which is akin to a gravure roll emerging from an ink tray, also yields selective filling of the cells (i.e., filled cells with no ink on the lands) in the presence of the wettability contrast pattern (Figure S1, Supporting Information). Selective filling by the guided drop and dip-coating methods is much slower than conventional gravure printing and represents a challenge for the future. Lowering the ink viscosity is one way to speed up the process; however, high solid loading is also desired. One general idea for increasing the filling rate is to deploy the ink on the pattern as a spray.

To directly observe the extent of selective cell filling, the silicon gravure pattern is filled with ink, rapidly frozen in a liquid cryogen, fractured under liquid nitrogen, and then imaged using cryoSEM. CryoSEM imaging of high-resolution gravure cells gives more information than indirect evidence from printed patterns. With no wettability contrast (i.e., features created in a silicon wafer with no coatings or silane treatments), selective filling of the cells is not possible. A wettability contrast between the hydrophobic lands and hydrophilic cell interiors is needed to have selective filling without doctoring. The magnitude of the wettability contrast is important to achieving this selective filling. Figure 2c,d shows cross-sectional cryoSEM images that demonstrate incomplete filling of patterns with a wettability contrast

of $\Delta\theta = 50^\circ$ and complete filling when a higher wettability contrast ($\Delta\theta = 80^\circ$) is achieved. Internal scallop features related to the etching treatment did not influence cell filling. Incomplete filling of the lower wettability contrast patterns was also evident in cells filled with nanoparticle ink (Figure S2, Supporting Information). With high wettability contrast, a wide range of cell geometries, including those less than $1\ \mu\text{m}$, could be selectively filled (Figures S3 and S4, Supporting Information).

CryoSEM data reveal that the extent of filling depends on the cell size. Namely, after ink filling, the smallest cells are underfilled (see Figure 2e), while the larger cells are overfilled (Figure 2g). A systematic study of these effects is provided in Figure S4 (Supporting Information). We suspect that pressure gradients associated with local meniscus curvature near the cells during ink loading might be responsible for the underfilling, but more work is needed to completely understand this phenomenon. Over- or underfilling of the cells is one factor that affects ink transfer during printing, as shown in Figure 2e–h. As demonstrated in Figure 2h, $\approx 90\%$ ink transfer occurred on printing from the overfilled cell, while less ink is transferred from the smaller, underfilled cell (Figure 2f). It should also be noted that ink transfer during printing has been actively studied by experiment^[17–19] and simulation^[20–23] and is influenced by various parameters such as substrate, nip pressure, print speed, and ink properties. Data for ink transfer, gathered from cryoSEM images, are provided in the Supporting Information (Figure S5). For a given cell depth, ink transfer increases as the cell width increases.

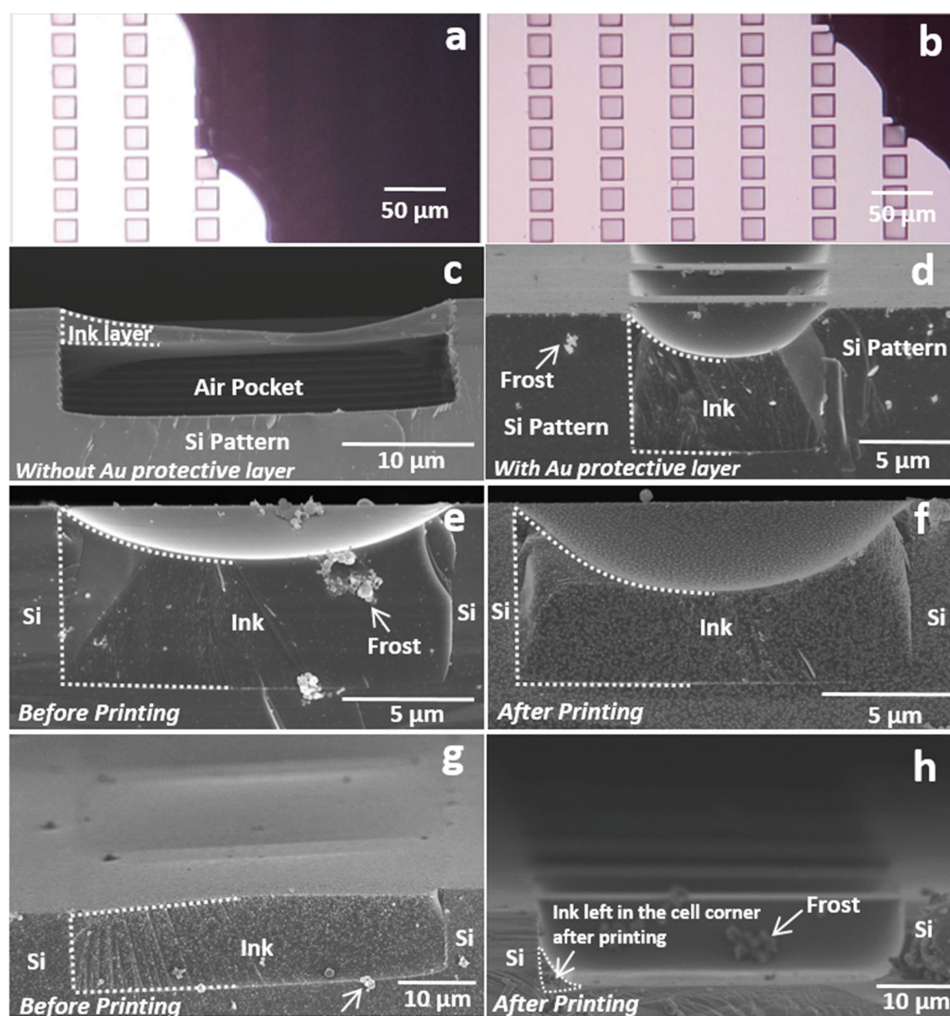


Figure 2. a,b) Time sequence optical microscope pictures of ink loading process by guiding a drop of a 80 wt% glycerol–20 wt% water solution over the pattern toward the upper right corner. c) CryoSEM image of a cell with a wettability contrast between hydrophobic land and hydrophilic cell of $\Delta\theta = 50^\circ$ after guided drop loading of a glycerol–water solution. d) CryoSEM image of a cell with a higher wettability contrast of $\Delta\theta = 80^\circ$ after guided drop loading of glycerol–water. CryoSEM images of a 15 μm wide cell e) after guided loading and f) after printing. CryoSEM images of a 50 μm guided loading cell g) before and h) after printing. Printing was carried out using a Kapton substrate with a 39° contact angle and a printing speed of 10 mm s^{-1} . Arrows point to frost formed during the cryoSEM specimen preparation.

Immediately after printing, the discrete transferred ink features spread and adjacent features merge to form continuous lines. With different substrates and treatments, features printed from the same gravure cells varied from discrete droplets on the least wettable substrates to overspread patches on the most wettable; intermediate wettability (e.g., PET with a contact angle of 19°) produced well defined, continuous lines (Figure S6, Supporting Information). Other factors that affect the merging of the discrete features into continuous line are the distance between adjacent cells (Figure S7, Supporting Information) and the action of the nip (Figure S8, Supporting Information). Suitable conditions for aqueous nanoparticle inks are chosen based on these observations.

Figure 3a shows a plot of printed silica line width and height as a function of the cell width. The printed line width was about 1.2–2 times of the cell width, indicating that some spreading occurs after deposition. This spreading behavior is

similar to that reported in the literature^[2,4,10] and drives the transition from discrete to continuous features. The height of the printed lines increased with cell width, indicating greater ink transfer. (See also Figure S5 in the Supporting Information.) A complicated silica nanoparticle pattern was used to probe the limits of high-resolution printing with nanoparticle inks. A representative printed pattern composed of 9 μm wide lines that are spaced as closely as 7 μm is shown in Figure 3b.

Figure 3c–i shows a series of printed silica lines with different final line width and spacing. These printed features are created from Si gravure patterns having different cell widths and spacings, whose patterns result in continuous lines at a 90° angle, a key requirement for conductive electrodes in printed circuits. The highest resolution achieved by this method to-date is 1.2 μm wide lines with a 1.5 μm spacing between them, as shown in Figure 3i and Figure S9 (Supporting Information). These fine printed features demonstrate

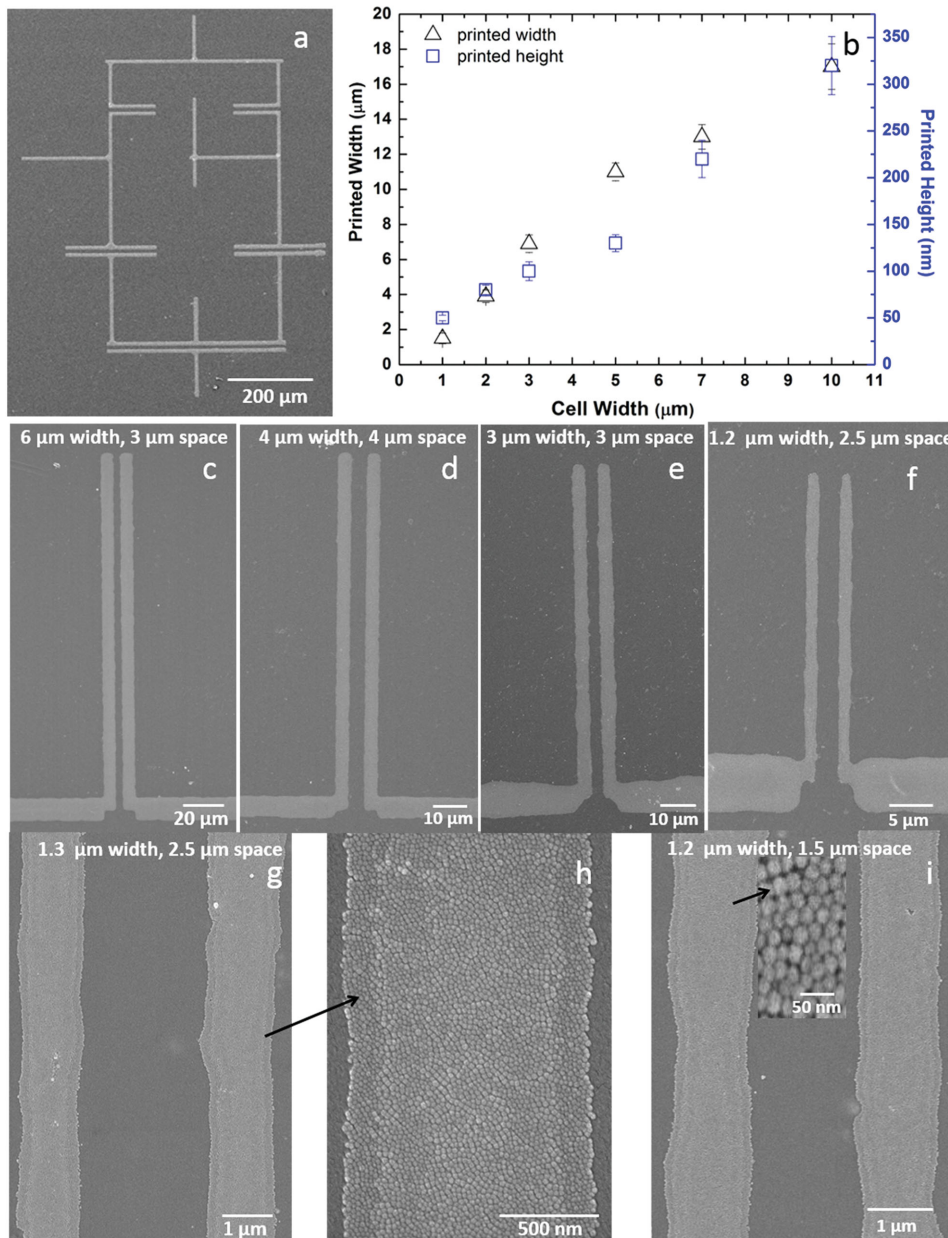


Figure 3. a) SEM image of a gravure printed complex pattern with 9 μm line width and 7 μm space between lines printed with silica nanoparticle ink. b) Plot of printed silica line width and height as a function of cell width. For data in panel (b), the cell depth was 5 μm, the printing speed 10 mm s⁻¹, and the substrate PET with contact angle of 19°. The error bar is based on at least five samples per data point. c–g) SEM images of printed lines with various line widths and spaces between lines; the images show no residual ink left on the space between the lines. h) High-magnification SEM image of panel (g) showing 1.3 μm wide silica. i) SEM image and high-magnification inset showing 1.2 μm wide silica lines with 1.5 μm space between them. For panels (c–i), the cell depth was 3.5 μm, the printing speed 10 mm s⁻¹, and the substrate PET with contact angle of 19°.

that the underfilling of the smaller cells does not necessarily hinder printing if adequate nip pressure is used (see Figure S8, Supporting Information).

Conductive electrode patterns for organic thin film transistors (OTFT) are also printed using the aqueous-based silver nanoparticle ink (Figure 4a). Silver lines with about ≈20 μm width were printed. Finer lines were not possible with this ink due to particle size, which is ≈200 nm as compared to 20 nm for the silica ink. The measured resistivity of a 350 nm thick,

50 μm wide printed silver line is $1.3 \times 10^{-5} \Omega \text{ cm}$, which is about an order of magnitude higher than bulk silver. Figure 4c shows an optical microscope picture of a printed OTFT based on gravure printed silver lines as source and drain electrodes. The OTFT employs poly(3-hexylthiophene) (P3HT) as the semiconductor, high-capacitance ion gels as the gate dielectric, and PEDOT:PSS as the top gate electrode.^[24] All the other components are aerosol-jet printed after the silver source/drain electrodes are gravure printed.^[25] An SEM image of this

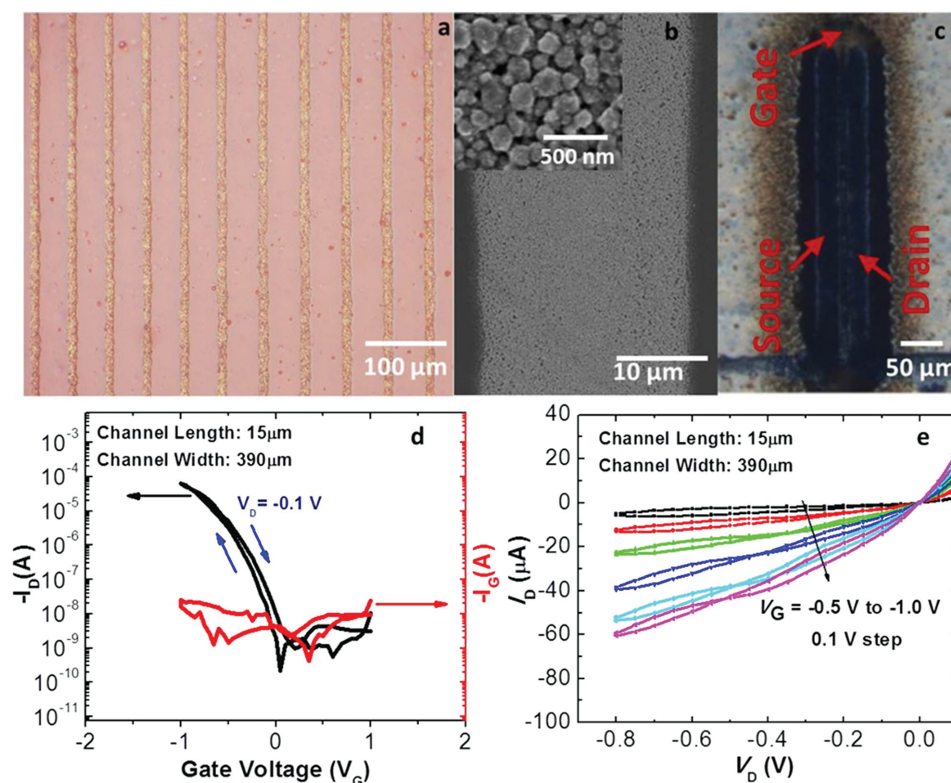


Figure 4. a) Optical microscope image of printed silver lines on Kapton. b) SEM image of gravure printed silver source and drain after annealing at 200°C for 1 h. c) Optical microscope image of an OTFT with gravure printed source and drain and aerosol-jet printed semiconductor (P3HT), ion gel dielectric, and PEDOT gate. d,e) I_D - V_G and I_D - V_D curves for the fully printed OTFT.

device is shown in Figure 4b. The electrical characteristics of the OTFT are shown in Figure 4d,e. The device channel length and width are 15 μm and 390 μm , respectively, and the average thickness of the silver line is 300 nm. The on/off current ratio was 10^5 with a high hole mobility $\approx 1 \text{ cm}^2 \text{ V}^{-1} \text{ s}^{-1}$. In addition, the P3HT TFT is also characterized by low gate leakage (in the nA regime), sharp onset, negligible hysteresis, and ohmic contacts as evidenced from linear I_D - V_D relation at low bias. All of these device characteristics are well matched to those of optimized electrolyte-gated P3HT TFT, as reported previously.^[26,27] These results demonstrate that the gravure method is promising for fabrication of low-voltage, high-performance OTFTs. Higher resolution features comparable to those printed with the silica ink are expected upon further optimization of the silver ink.

In summary, we have demonstrated a high-resolution, gravure printing method based on using patterned silicon wafers with engineered wettability contrast. By independently tailoring the wetting behavior of the cells and land regions, we have achieved gravure printing without the need for doctor blading. Conductive silver electrodes with 15 μm channel length in OTFT device and continuous silica nanoparticle lines as narrow as 1.2 μm with 1.5 μm spaces have been printed by this new method.

Experimental Section

Materials: All photolithography was done using 10 cm (100) silicon wafers. The flexible silicon was fabricated by immersing standard

wafer into 25% KOH bath until required thickness is reached. Trichloro(1H,1H,2H,2H-perfluorooctyl) silane FOTS was from Sigma-Aldrich. The substrates were polyimide (Kapton, Dupont) and polyethylene terephthalate (PET, 3M). Substrate surface energies were adjusted with plasma treatment.

The model ink was 80 wt% glycerol–20 wt% water solution with a viscosity of 47 cP. A silica nanoparticle ink (average particle size of ≈ 20 nm) was prepared by mixing an aqueous dispersion (Ludox TMA, Sigma-Aldrich) with glycerol. The silica loading is ≈ 40 wt% and the viscosity is 120 cP with no shear thinning. The silver nanoparticle ink was synthesized by a procedure reported elsewhere.^[28] The 77 wt% silver ink (average particle size of ≈ 200 nm) was mixed with glycerol to reach a solids loading of 30 wt%. The viscosity is 400 cP at 1 s^{-1} , and shear thinning was observed (1100 cp at 0.01 s^{-1} and 200 at 1000 s^{-1}).

Gravure Pattern Fabrication: The pattern was fabricated by standard photolithography. The patterned silicon wafer was then dry etched to required depth (SLR-770). Before removing photoresist, a 50 nm layer of nickel was deposited by e-beam evaporator (CHA-SEC-600). The wafer was then washed in acetone to remove the photoresist and the excess nickel coating on it. The patterned wafer with nickel layer in the cell was exposed to FOTS vapor for 12 h.

Improved wettability contrast was achieved by the following modification. After nickel layer deposition, a 15 nm coating of gold was deposited by e-beam evaporation. The photoresist, nickel, and gold coating were removed by a lift-off procedure, leaving silicon oxide on the lands and gold covering nickel layer in the cells. After the FOTS treatment, the gold layer was removed by gold etcher (GE-6) to expose fresh nickel surface.

Ink Loading: In guided method, a drop of ink was dispensed onto the patterned wafer and the ink drop was dragged over the pattern. In dip-coating method, the silicon gravure pattern was dipped into the ink reservoir and withdrawn from the ink using a computer-controlled dip-coating system.

Characterization: The contact angle was measured by sessile drop method. Optical images and video were obtained by a digital optical microscope (Hirox MX series). SEM images were obtained with scanning electron microscopy (S-4700, Hitachi).

Cryo-SEM: A piece of silicon pattern ($1 \times 1 \text{ cm}^2$) after the process stage of interest was plunged into a liquid nitrogen bath. The liquid shape was at equilibrium before plunging and cooling rates in plunge freezing were on the order of 1000 K s^{-1} .^[29] The silicon wafer was mounted on a specially designed carrier and was broken in the liquid nitrogen to expose the cross section of the cells. The sample carrier was screwed onto a cryo-transfer rod (Emitech, Kent, UK), which was immediately inserted into a preparation chamber (Emitech K-1250, Kent, UK) for conductive metal coating. The platinum coated sample was then transferred to a Hitachi S-4700 scanning electron microscope for examination. The sample was kept around $-150 \text{ }^\circ\text{C}$ by a liquid-nitrogen-cooled stage during imaging. Aside from frost contamination, no other freezing artifacts were noted.

Printing: In roll-to-roll printing mode, a patterned flexible silicon wafer was wrapped around a roller. The gap between the rolls was adjustable and the rotation speeds of the two rolls were controlled by a computer. The substrate was fed between the two rolls during printing. In the flat patterned wafer mode, the substrate was wrapped around a roll, a flat patterned wafer was loaded with ink and then fed through between the two rolls as in Figure 1d. Patterns were used over many print runs without a noticeable loss in performance.

Device Fabrication and Characterization: P3HT was from Rieke Metals. The ion gel ink was composed of 1.0 wt% polystyrene-*b*-poly(methylmethacrylate)-*b*-poly(styrene) and 9 wt% of ionic liquid ((1-ethyl-3-methylimidazolium bis(trifluoromethylsulfonyl)amide, Merck) in ethyl acetate solution. Poly(3,4-ethylenedioxythiophene) poly(styrenesulfonate) ink (Starck) was diluted with 10% of ethylene glycol. Silver source/drain contacts were printed on Kapton by gravure printing using silver nanoparticle ink, and then annealed at $200 \text{ }^\circ\text{C}$ for 1 h. Printing of P3HT, ion gel, and PEDOT:PSS inks was accomplished using an aerosol-jet printing system (Optomec). Completed devices were annealed at $120 \text{ }^\circ\text{C}$ for 1 h before transferring to a nitrogen-filled glove box where the electrical measurements were performed using Keithley 236/237 source meters and 6517A high-impedance electrometers.

Supporting Information

Supporting Information is available from the Wiley Online Library or from the author.

Acknowledgements

This work was supported by the Multi-University Research Initiative (MURI) program sponsored by the Office of Naval Research (MURI Award N00014-11-1-0690) and the L.E. Scriven Chair at the University of Minnesota. Parts of this work were carried out at the Characterization Facility and the Nanofabrication Center of the University of Minnesota.

Received: June 2, 2015

Revised: August 29, 2015

Published online: October 19, 2015

- [1] M. M. Voigt, A. Guite, D. Chung, R. U. A. Khan, A. J. Campbell, D. D. C. Bradley, F. Meng, J. H. G. Steinke, S. Tierney, I. McCulloch, H. Penxten, L. Lutsen, O. Douheret, J. Manca, U. Brokmann, K. Soennichsen, D. Huelsenberg, W. Bock, C. Barron, N. Blanckaert, S. Springer, J. Grupp, A. Mosley, *Adv. Funct. Mater.* **2010**, *20*, 239.
- [2] E. Hrehorova, M. Rebros, A. Pekarovicova, B. Bazuin, A. Ranganathan, S. Garner, G. Merz, J. Tosch, R. Boudreau, *J. Disp. Technol.* **2011**, *7*, 318.
- [3] A. Pierre, M. Sadeghi, M. M. Payne, A. Facchetti, J. E. Anthony, A. C. Arias, *Adv. Mater.* **2014**, *26*, 5722.
- [4] H. Kang, R. Kitsomboonloha, J. Jang, V. Subramanian, *Adv. Mater.* **2012**, *24*, 3065.
- [5] S. Tekoglu, G. Hernandez-Sosa, E. Kluge, U. Lemmer, N. Mechau, *Org. Electron.* **2013**, *14*, 3493.
- [6] G. Hernandez-Sosa, N. Bornemann, I. Ringle, M. Agari, E. Doersam, N. Mechau, U. Lemmer, *Adv. Funct. Mater.* **2013**, *23*, 3164.
- [7] H. Kempa, M. Hamsch, K. Reuter, M. Stanel, G. C. Schmidt, B. Meier, A. C. Huebler, *IEEE Trans. Electron Devices* **2011**, *58*, 2765.
- [8] D. A. Alsaïd, E. Rebrosova, M. Joyce, M. Rebros, M. Atashbar, B. Bazuin, *J. Disp. Technol.* **2012**, *8*, 391.
- [9] E. B. Secor, S. Lim, H. Zhang, C. D. Frisbie, L. F. Francis, M. C. Hersam, *Adv. Mater.* **2014**, *26*, 4533.
- [10] D. Sung, A. d. I. F. Vornbrock, V. Subramanian, *IEEE Trans. Compon. Packag. Technol.* **2010**, *33*, 105.
- [11] M. Pudas, J. Hagberg, S. Leppavuori, *J. Eur. Ceram. Soc.* **2004**, *24*, 2943.
- [12] R. Kitsomboonloha, S. J. S. Morris, X. Rong, V. Subramanian, *Langmuir* **2012**, *28*, 16711.
- [13] R. Kitsomboonloha, V. Subramanian, *Langmuir* **2014**, *30*, 3612.
- [14] V. Subramanian, J. Cen, A. d. I. F. Vornbrock, G. Grau, H. Kang, R. Kitsomboonloha, D. Soltman, H. Tseng, *Proc. IEEE* **2015**, *103*, 567.
- [15] F. R. Pranch, D. J. Coyle in *Liquid Film Coating*, (Eds: S. F. Kistler, P. M. Schweizer), Chapman & Hall, New York **1997**, pp. 599–635.
- [16] T. Velten, F. Bauerfeld, H. Schuck, S. Scherbaum, C. Landesberger, K. Bock, *Microsyst. Technol.* **2011**, *17*, 619.
- [17] X. Yin, S. Kumar, *Chem. Eng. Sci.* **2006**, *61*, 1146.
- [18] H. W. Kang, H. J. Sung, T. Lee, D. Kim, C. Kim, *J. Microchem. Microeng.* **2009**, *19*, 015025.
- [19] H. K. Chuang, C. C. Lee, T. J. Liu, *Int. Polym. Process.* **2008**, *23*, 216.
- [20] D. M. Campana, M. S. Carvalho, *J. Fluid Mech.* **2014**, *747*, 545.
- [21] S. Dodds, M. S. Carvalho, S. Kumar, *Phys. Fluids* **2009**, *21*, 092103.
- [22] W. Huang, S. Lee, H. J. Sung, T. Lee, D. Kim, *Int. J. Heat Fluid Flow* **2008**, *29*, 1436.
- [23] S. Dodds, M. S. Carvalho, S. Kumar, *J. Fluid Mech.* **2012**, *707*, 521.
- [24] S. H. Kim, K. Hong, W. Xie, K. H. Lee, S. Zhang, T. P. Lodge, C. D. Frisbie, *Adv. Mater.* **2013**, *25*, 1822.
- [25] J. H. Cho, J. Lee, Y. Xia, B. Kim, Y. He, M. J. Renn, T. P. Lodge, C. D. Frisbie, *Nat. Mater.* **2008**, *7*, 900.
- [26] Y. Xia, W. Zhang, M. Ha, J. H. Cho, M. J. Renn, C. H. Kim, C. D. Frisbie, *Adv. Funct. Mater.* **2010**, *20*, 587.
- [27] S. H. Kim, K. Hong, K. H. Lee, C. D. Frisbie, *ACS Appl. Mater. Interfaces* **2013**, *5*, 6580.
- [28] B. Y. Ahn, E. B. Duoss, M. J. Motala, X. Guo, S. Park, Y. Xiong, J. Yoon, R. G. Nuzzo, J. A. Rogers, J. A. Lewis, *Science* **2009**, *323*, 1590.
- [29] J. A. N. Zasadzinski, *J. Microsc.* **1988**, *150*, 137.